Variance Analysis of Incoherent Integration Applied to Simulated Equatorial Electrojet Irregularities Radar Power Spectra

H. C. Aveiro* [(1)], C. M. Denardini [(1)], M. A. Abdu [(1)], N. J. Schuch[(2)], L. C. A. Resende[(1,3)], P. D. S. C. Almeida[(1,3)].

[(1)] Instituto Nacional de Pesquisas Espaciais - P. O. Box 515 - S. J. Campos, SP, Brasil.
[(2)] Instituto Nacional de Pesquisas Espaciais - Centro Regional Sul de Pesquisas Espaciais - Santa Maria, RS, Brasil.
[(3)] ETEP Faculdades - Av. Br. do Rio Branco, 882 - 12242-800 - S. J. Campos - SP, Brasil.

Abstract

The spectral analysis of the received echoes from equatorial electrojet irregularities may show the signatures of two different plasma irregularities: Type 1 and Type 2. Each Type is related to a distinct process of plasma instabilities. Each irregularity presents itself as one gaussian-like shape in the frequency domain and the characteristics of the curve may be extracted using nonlinear curve fitting methods. Some techniques are applied to the irregularities spectra before the curve fitting so that the variance between the data and the fitting is minimum. One of these techniques is called incoherent integration and consists of averaging subsequent spectra. We simulated equatorial electrojet radar power spectra of Type 1 irregularities to elucidate the effects. The advantages and disadvantages of applying such technique are analyzed in terms of the variance between the radar spectra and the fitted curve.

Introduction

The region between 90 and 120 km of altitude (at the ionospheric E region heights) in the latitudinal range of ±3º around the dip equator presents one intense electric current, denominated equatorial electrojet, EEJ (Forbes, 1981). It is driven by the E region dynamo (Fejer and Kelley, 1980) and it has an important role in the phenomenology control of the ionosphere-thermosphere system. The EEJ was initially detected in the first half of the twentieth century as geomagnetic large scale variations in magnetic observatories close to the equator. Egedal (1948) was the first one to conclude that this variation was due to an electric current flow under the magnetic dip equator; however, it was Chapman (1951) who first explained it, terming this phenomenon as equatorial electrojet.

Studies of the equatorial ionosphere using VHF radars have shown backscattered echoes from electron density irregularities in the EEJ. These studies showed distinct spectral signatures of two types of irregularities, called Type 1 and Type 2, explained by a modified two-stream (Farley, 1963; Buneman, 1963) and the gradient drift (Rogister and D'Angelo, 1970) instabilities, respectively. Several experiments have been done to investigate the EEJ irregularities in order to characterize its spectra and explain the phenomenology in many sectors, such as Peruvian (Cohen and Bowles, 1967; Balsley, 1969; Cohen, 1973; Fejer et al., 1975; Farley and Fejer, 1975), Indian (Prakash et al., 1971; Reddy and Devasia, 1981), and Brazilian (Abdu et al., 2002; Abdu et al., 2003; de Paula and Hysell, 2004; Denardini et al., 2004; Denardini et al., 2005).

In the Brazilian sector a 50 MHz coherent backscatter radar, also known by the acronym RESCO (in Portuguese, *Radar de ESpalhamento COerente*), has been operated since 1998 at São Luís, (2.33° S, 44.2° W, DIP: -0.5), on the dip equator. Observations of EEJ 3-m plasma irregularities are routinely carried out with the main purpose of studying the EEJ dynamics through spectral analysis of the backscattered echoes from plasma instabilities. For such studies, a precise determination of the spectral moments of the irregularities is a crucial requirement. Several techniques for estimating Doppler shifts based on radar power spectra have been reviewed and compared (May, 1989a; May, 1989b; Woodman, 1985). The RESCO radar data processing usually estimates the irregularity Doppler shifts by fitting two Gaussians to each power spectrum using the Non-Linear Least Squares Fitting Method (Levenberg, 1944; Marquardt, 1963; Press et al., 1992). The perfomance of the fitting method depends on the variance of the spectral noise power. The technique of incoherent integration presents itself as a good tool to reduce variance of the noise without changing the mean spectral densities of both signal and noise (Fukao, 1989). Increasing the number of integrated spectra means to reduce the variance and to define better the power spectra.

We have applied the technique to simulated radar backscattered power spectra of Type 1 equatorial electrojet irregularities. We quantified the advantages and disadvantages of applying such technique. The following sections present the typical radar data processing, a brief description of the spectra simulations, and the results of this statistical study, which are discussed in terms of the variance of the estimate Type 1 Doppler frequency.

Data Generation, Incoherent Integration and Moment Estimation

The RESCO radar is operated routinely during two weeks per month. It is usually set for EEJ sounding transmitting one pulse each 1-2 ms with pulse width of 20 μs and time delay of 600 μs. Therefore, the power spectra within the

Doppler frequencies, related to the Doppler shift, obtained from Fast Fourier Transform (FFT), have an aliasing frequency of 250-500 Hz. The frequency resolution is determined by the number of subsequent pulses taken for the FFT analysis and by the aliasing frequency. From each spectrum, seven parameters are estimated through curve fitting. The RESCO data processing usually fits the sum of two Gaussian curves to the spectrum, each one related to one irregularity type.

Once the focus of the work is the study of type 1 irregularity spectra, the Gaussian covariance model of Zrnic (1979) was used to simulate power spectra of 3-meters plasma irregularities containing only the characteristics of the Farley-Buneman instability. Type 1 power spectra were simulated having 256 points each one. All these spectra were chosen to have f_d = 120 Hz and σ=20 Hz. The white noise was added to the data in time domain in order to assure a more realistic variance in the power spectra. So, each spectrum simulated is described by a noise level added to a Gaussian curve (Takeda et al., 2001), i.e., our data set was described by one function *S* in relation to the frequency *f*, given by:

$$S(f) = \frac{P}{\sigma\sqrt{2\pi}} \exp\left[-\frac{(f-f_d)^2}{2\sigma^2} \right] + P_N \quad , \qquad (1)$$

where P, f_d, σ and P_N are, respectively, the spectral power, the center of frequency distribution (corresponding to the Doppler shift), spectral width and noise level. An example of a spectrum simulated is presented in Figure 1 where the quantities mentioned above are indicated in different colors. The green dashed line represents the noise power density (P_N), the vertical red line shows the center of frequency distribution (f_d), the difference between the vertical orange and red lines determines the standard deviation of the curve fitted to the power spectrum and the area between the blue dashed line and the green dashed line defines the power of the signal (P) (Aveiro et al., 2007).

We started step two analyzing the simulated power spectra after having a proper data set with *a priori* Type 1 characteristics from which we could establish comparison with the parameters estimated by the method. To reduce our data set of 256 points to 4 parameters, we have used the Maximum Likelihood Estimator (MLE) with the purpose of minimize the square sum of residual error as given by (Woodman, 1985):

$$\varepsilon^2 = \sum_{i=1}^{N} \left[y_i - S(f_i; P, f_d, \sigma) \right]^2 \quad , \qquad (2)$$

where N is the number of frequency points and y_i is the observed spectral amplitude for one given frequency.

Despite curve fitting algorithm being largely used, it usually does not present results satisfactory enough when the variance is too high. A solution to reduce variances is to integrate incoherently several consecutive spectra. The method consists in averaging the power spectral density at a given frequency from several consecutive spectra, for all frequencies in the spectrum. Since the white noise is a random component, the resulting spectrum will have lower variance. Figure 2 presents an illustration of the resulting spectrum (on the right side) from incoherent integration of hundred consecutive spectra (on the left side), where a noisy bunch of spectra (represented by the first one) became a smoothed one (Aveiro et al, 2007). The incoherent integration reduces the variance of the noise (σ_N^2) and better defines the power spectra, but it does not change the mean values of signal (P) and noise spectral (P_N) densities (Fukao, 1989). In a spectrum

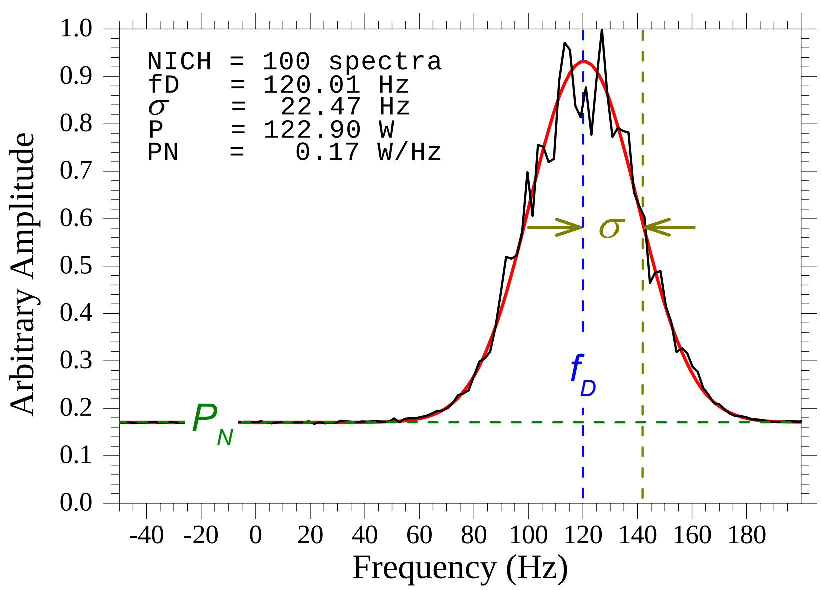

Figure 1 – Power spectrum resulting from the incoherent integration of one hundred simulated power spectra (black line) superimposed by a Gaussian curve (red line) fitted to the spectrum using Least Square Error Method. The green line represents the noise power density (P_N), the vertical blue line shows the center of frequency distribution (f_d), the difference between the vertical brown and blue lines determines the standard deviation of the Gaussian curve fitted to the spectrum (σ) and the area between the red and the green line defines the power of the signal (P) (After Aveiro et al, 2007).

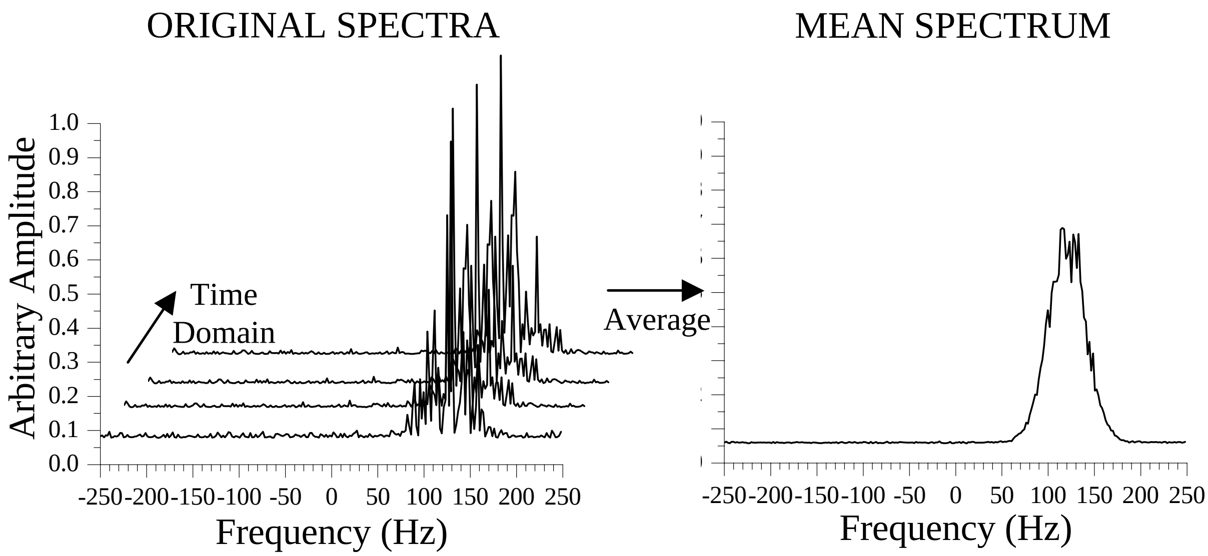

Figure 2 – Illustration of incoherent integration applied to hundred consecutive spectra (left) and the resultant spectrum (right) (After Aveiro et al, 2007).

without incoherent integration, σ_N is equal to P_N. But, the unitary ratio σ_N/P_N decays with the inverse of the square root of the number of incoherent integrations (*NICH*), i.e., σ_N becomes equal to the relation $P_N/(NICH)^{1/2}$.

The Gaussian covariance model of Zrnic (1979) was used to simulate groups of Gaussian-like power spectra with the characteristics described above (f_d = 120 Hz and σ=20 Hz). Each group had one different signal-to-noise ratio (*SNR*): 1, 2, 4, 6, 8, 10, 20, 40, 60, 80 and 100 dB. Theses groups were arranged and those spectra were integrated incoherently in such a way that we always have one thousand power spectra per group with one different value of *NICH*: 1, 2, 4, 6, 8, 10, 20, 40, 60, 80 and 100. Thus, we obtained 121 sub-groups allowing independence between our results and, *NICH* and *SNR*. The data sets of power spectra simulated were processed as ordinary spectra obtained in the RESCO data processing. We have used MLE to minimize the square sum of residual error in a way to fit a Gaussian (Eq. 2). The same algorithm has fitted each spectrum of the 121 data sets to a single Gaussian. The analysis consisted of the comparison of the estimate parameters variance in function of *SNR* and *NICH*.

Results and Discussions

The analysis of the variances of the estimate moments gives us an indication of the accuracy of each parameter for the given *SNR*. Table 1 shows that the higher the *NICH* the lower the variances. A clear example is the highest variances of σ when no incoherent integration is applied. It also presents that the higher the *SNR* the lower the variances. Those indicates that the curve fitting hardly ever have good estimates for this parameter (Aveiro et al., 2007).

Our results had shown that increasing *NICH* from 1 to 100 spectra results in 100 times reduction in the variance of f_d, which in turn increased the confidence of the Doppler velocity of the plasma irregularity. However, the application of the technique means longer observational time. For example, in case of incoherently integrating 10 spectra the observational time is worsened by a factor of 10, i.e., the observational time increases directly proportional to the number of spectra used in the integration.

Other point we would like to address in this paper is the dependence of the average variance of f_d (VAR_{fd}) from the number of integrated spectra (*NICH*). Our results (not presented in graphical format) shows a linear dependence between the natural logarithmic of variance of f_d and the natural logarithmic of the incoherent integrations as described by Aveiro et al (2007). In order to quantify the dependences for the different *SNR*'s, we have performed a linear fitting to these data in ln-ln domain, fiitting the following equation to the data:

$$VAR_{fd} = NICH^{\varepsilon} \cdot e^{\psi}, \qquad 1 \leq NICH \leq 100 \quad , \tag{3}$$

where VAR_{fd} is the fitted variance of estimate f_d, ε is the negative power coefficient that tell us how much the VAR_{fd} reduces as we increase the *NICH*, and the exponential of ψ is the VAR_{fd} observed when no incoherent integration is applied. Table 2 presents the values of ε, ψ e *R* in function of *SNR* and *NICH*.

Table 2 also shows that the parameter ε is aproximatelly independent from *SNR* and *NICH*. This term, ε, is almost unitary, demonstrating that VAR_{fd} is inversely proportional to *NICH*. The lower the ψ the higher the *SNR* was analysed and quantified. The linear mathematical relation between the natural logarithms (blue dots) is presented in Figure 3. In order to quantify the dependence, we have performed a linear fitting to these data in ln-ln domain, represented by the red curve superimposed to the graph on Figure 3. The following equation has been used to fit the data:

$$\psi = SNR^{\alpha} \cdot e^{\beta}, \qquad 1 \leq SNR \leq 100 . \quad , \tag{4}$$

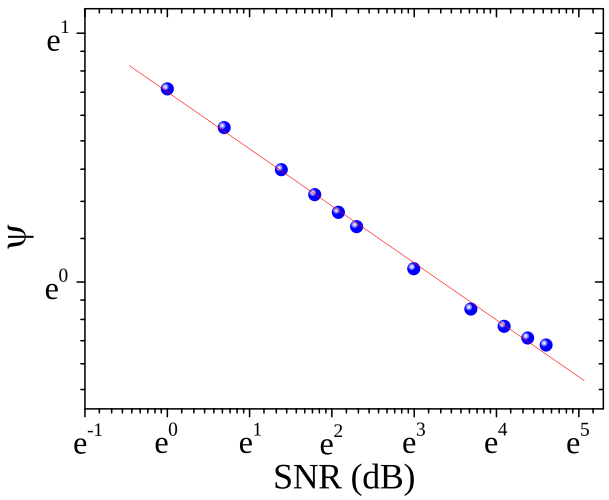

Fig. 3 – ψ in function of the number spectra used in the incoherent integrations (*NICH*). The analyzed points are the blue dots and the logarithmical fitting is the red curve.

The power coefficient α resulted –0.2293 (±0.00416). The *β* factor resulted 0.76434 (±0.01221). And the correlation coefficient *R* resulted –0.99853. Unifying Eqs. (3) and (4), we have the variance of VAR_{fd} in function of *SNR* and *NICH*, as given by:

$$VAR_{fd} = NICH^{\varepsilon} \cdot e^{e^{\beta} \cdot SNR^{\alpha}} . \quad (5)$$

Eq. (5) shows the behaviour of the variance of estimate f_d (VAR_{fd}) to some expected cases:

- with no incoherent integration (*NICH*=1), the variance will depend only from the signal-to-noise ratio; and
- the higher the NICH the lower the variance.

Although all the benefits that incoherent integration gives, we shall be careful with the time resolution of our data. For example, incoherently integrate 10 spectra means worsening 10 times the time resolution. Thus, in the case of one spectrum per 6 seconds, after the integration it would result one spectrum per 60 seconds. It means compromising between the number of incoherent integrations and time resolution. Higher values of *NICH* will always allow better values of variance, however could compromise the time escale of the data.

Conclusions

The technique of incoherent integration has shown to be a valuable tool, which is able to improve significantly the estimates of the test parameter (the center of the frequency distribution of the power spectra from the radar echoes of the EEJ irregularities). As a result of increasing the number of incoherently integrated spectra, the degree of success in estimating the test parameter is improved. We have shown in this paper the linear dependence of the natural logarithmic of variance of the estimate f_d and the natural logarithmic of the incoherent integration. The power coefficient ε from linear fitting indicated that increases in the number of spectra incoherently integrated will almost proportionally decrease the variance of the estimate Doppler frequency. In addition, we have found an exponential factor ψ, which it was shown to be related to SNR of the data set. Finally, we have seen that applying incoherent integrations to the observational radar spectra of Type 1 equatorial electrojet irregularities means to decrease the variance between the observational and estimate Doppler frequency when using MLE techniques, but we have to balance the variance of the estimate Doppler frequency and the observational time.

Acknowledgments

H. C. A. wishes to thank CNPq/MCT for financial support to their Msc program through the project nr. 131326/2007-4. L. C. A. R. and P. S. C. A. wish to thank CNPq/MCT for financial support to their undergraduate programs through the projects nr. 101536/2006-2 and 105374/2005-9, respectively.

References

ABDU, M. A., DENARDINI, C. M., SOBRAL, J. H. A., BATISTA, I. S., MURALIKRISHNA, P. & DE PAULA, E. R., 2002, Equatorial electrojet irregularities investigations using a 50 MHz back-scatter radar and a Digisonde at São Luís: Some initial results: Journal of Atmospheric and Solar-Terrestrial Physics, Vol. 64, No. 12-14, p.1425-1434.

ABDU, M. A., DENARDINI, C. M., SOBRAL, J. H. A., BATISTA, I. S., MURALIKRISHNA P., IYER, K. N., VELIZ, O. & DE PAULA, E. R., 2003, Equatorial electrojet 3 m irregularity dynamics during magnetic disturbances over Brazil: results from the new VHF radar at São Luís: Journal of Atmospheric and Solar-Terrestrial Physics, Vol. 65, No. 14-15, p.1293-1308.

AVEIRO, H. C., DENARDINI, C. M., ABDU, M. A., SCHUCH, N. J., 2007, Statistical Study of Incoherent Integration Applied to Simulated Power Spectra of Radar Signals Backscattered from Equatorial Electrojet Irregularities: Brazilian Journal of Geophysics (in press).

BALSLEY, B.B., 1969, Some Characteristics of Non-2-Stream Irregularities in Equatorial Electrojet, Journal of Geophysical Research, Vol. 74, p.2333-2347.

BUNEMAN, O., 1963. Excitation of field aligned sound waves by electron streams: Physical Review Letters, Vol. 10, No. 7, p.285-287.

CHAPMAN, S., 1951, The equatorial electrojet as detected from the abnormal electric current distribution about Huancayo, Peru and elsewhere: Archives Fur Meteorology, Geophysics and Bioclimatology, A44, p.368-390.

COHEN, R., AND K.L. BOWLES, 1967, Secondary Irregularities in Equatorial Electrojet, Journal of Geophysical Research, Vol. 72, p.885-894.

COHEN, R., 1973, Phase Velocities of Irregularities in Equatorial Electrojet, Journal of Geophysical Research, Vol. 78, p.2222-2231.

DE PAULA, E.R., AND D.L. HYSELL, 2004, The Sao Luis 30 MHz coherent scatter ionospheric radar: System description and initial results, Radio Science, Vol.39, No. 1, p.1-11.

DENARDINI, C. M., ABDU, M. A. & SOBRAL, J. H. A., 2004, VHF radar studies of the equatorial electrojet 3-m irregularities over São Luís: day-to-day variabilities under auroral activity and quiet conditions: Journal of Atmospheric and Solar-Terrestrial Physics, Vol. 66, n17, p.1603-1613.

DENARDINI, C.M., M.A. ABDU, E.R. DE PAULA, J.H.A. SOBRAL, AND C.M. WRASSE, 2005, Seasonal characterization of the equatorial electrojet height rise over Brazil as observed by the RESCO 50 MHz back-scatter radar, Journal of Atmospheric and Solar-Terrestrial Physics, Vol. 67, No. 17-18, p.1665-1673.

EGEDAL, J., 1948, Daily variation of the horizontal magnetic force at the magnetic equator: Nature, Vol. 161, p.443-444.

FARLEY, D. T., 1963, A plasma instability resulting in field aligned irregularities in the ionosphere: Journal of Geophysical Research, Vol. 68, No. A22, p.6083-6097.

FARLEY, D.T., AND B.G. FEJER, 1975, The Effect of Gradient Drift Term on Type 1 Electrojet Irregularities, Journal of Geophysical Research, Vol. 80, p.3087-3090.

FEJER, B.G., D.T. FARLEY, B.B. BALSLEY, AND R.F. WOODMAN, 1975, Vertical Structure of VHF Backscattering Region in Equatorial Electrojet and Gradient Drift Instability, Journal of Geophysical Research, Vol. 80, p.1313-1324.

FEJER, B. G. & KELLEY, M. C., 1980, Ionospheric Irregularities: Reviews of Geophysics and Space Physics, Vol. 18, No. 2, p.401-454.

FORBES, J. M., 1981, The Equatorial Electrojet: Reviews of Geophysics and Space Physics, Vol. 19, No. 3, p.469-504.

FUKAO, S., 1989, Middle atmosphere program – Handbook for map: International school on atmospheric radar, Vol. 30, Urbana (IL): SCOSTEP Secretariat.

LEVENBERG, K., 1944, A Method for Solution of Certain Non-Linear Problems in Last Squares, Quarterly of Applied Mathematics, Vol. 2, No. 1, p.164-168.

MARQUARDT, D.W., 1963, An Algorithm for Least-Squares Estimation of Nonlinear Parameters, Journal of the Society for Industrial and Applied Mathematics, Vol. 11, No. 2, p.431-441.

PRESS, W. H., TEUKOLSKY, S. A., VETTERLING, W. T., FLANNERY, B. P., 1992, Numerical recipes in C**:** the art of scientific computing. 2. ed. Cambridge: Cambridge University Press.

MAY, P. T., SATO, T., YAMAMOTO, M., KATO, S., TSUDA, T. & FUKAO, S., 1989a, Errors in the Determination of Wind Speed by Doppler Radar: Journal of Atmospheric and Oceanic Technologies, Vol. 6, No. 2, p.235-242.

MAY, P. T. & STRAUCH, R.G., 1989b, An Examination of Wind Profiler Signal Processing Algorithms: Journal of Atmospheric and Oceanic Technologies, Vol. 6, No. 4, p.731-735.

PRAKASH, S., S.P. GUPTA, B.H. SUBBARAY, AND C.L. JAIN, 1971, Electrostatic Plasma Instabilities in Equatorial Electrojet, Nature (Physical Science), Vol. 233, No. 38, p.56-58.REDDY, C. A., 1981, The equatorial electrojet: a review of ionospheric and geomagnetic aspects: Journal of Atmospheric and Terrestrial Physics, Vol. 43, No. 5/6, p.557-571.

REDDY, C.A., AND C.V. DEVASIA, 1981, Height and Latitude Structure of Electric-Fields and Currents Due to Local East-West Winds in the Equatorial Electrojet, Journal of Geophysical Research, Vol. 86, p.5751-5767.

ROGISTER, A. AND D'ANGELO, N., 1970, Type 2 irregularities in the equatorial electrojet: Journal of Geophysical. Research, Vol. 75, p.3879-3887.

WOODMAN, R.F., 1985, Spectral moment estimation in MST radars: Radio Science, Vol. 20, No. 6, p.1185-1195.

ZRNIC, D. S., 1979, Estimation of spectral moments of weather echoes: IEEE Transactions of Geoscience on Electronics, Vol. 17, p.113-128.

Table 1 – Average variance of the estimate f_d in function of NICH and SNR.

NICH/SNR	1 dB	2 dB	4 dB	6 dB	8 dB	10 dB	20 dB	40 dB	60 dB	80 dB	100 dB
1	6.9583	6.0953	5.0198	4.4752	4.1749	3.9029	3.3258	2.8815	2.7962	2.7346	2.6996
2	5.0553	3.3786	2.4028	2.0283	1.8043	1.6743	1.3536	1.1484	1.0657	1.017	0.9926
4	2.4757	1.6096	1.1369	0.959	0.8608	0.7933	0.6396	0.5412	0.4988	0.4752	0.4605
6	1.6293	1.0576	0.7474	0.631	0.5628	0.5213	0.4208	0.3548	0.3272	0.312	0.3019
8	1.213	0.7888	0.5583	0.4689	0.4202	0.3886	0.3135	0.2645	0.2439	0.2322	0.2248
10	0.9658	0.6294	0.4443	0.3743	0.335	0.3095	0.2498	0.2107	0.1942	0.1849	0.1787
20	0.4798	0.3123	0.2206	0.1858	0.1666	0.1537	0.1241	0.1046	0.0964	0.0918	0.0887
40	0.2391	0.1555	0.11	0.0926	0.0829	0.0766	0.0619	0.0522	0.0481	0.0458	0.0442
60	0.1592	0.1036	0.0732	0.0617	0.0553	0.0511	0.0412	0.0348	0.032	0.0305	0.0294
80	0.1194	0.0777	0.0549	0.0463	0.0414	0.0383	0.0309	0.026	0.024	0.0228	0.0221
100	0.0954	0.0621	0.0439	0.037	0.0331	0.0306	0.0247	0.0208	0.0192	0.0183	0.0177

Table 2 – Parameters ε, ψ and R, in function of *SNR*.

SNR (dB)	ε	ψ	*R*
1	-0.97318	2.17306	-0.99808
2	-1.00728	1.85938	-0.99987
4	-1.02404	1.56969	-0.99989
6	-1.03042	1.41975	-0.99975
8	-1.03423	1.32224	-0.99960
10	-1.03582	1.24859	-0.99956
20	-1.04168	1.05430	-0.99928
40	-1.04538	0.89636	-0.99914
60	-1.05142	0.83575	-0.99882
80	-1.05481	0.79782	-0.99864
100	-1.05815	0.77545	-0.99851

10th International Congress of the Brazilian Geophysical Society

Promotion

SBGf

Master Sponsor

BR PETROBRAS

Supported by

anp Agência Nacional do Petróleo, Gás Natural e Biocombustíveis

CAPES

CNPq Conselho Nacional de Desenvolvimento Científico e Tecnológico

FAPERJ Fundação Carlos Chagas Filho de Amparo à Pesquisa do Estado do Rio de Janeiro

FINEP FINANCIADORA DE ESTUDOS E PROJETOS MINISTÉRIO DA CIÊNCIA E TECNOLOGIA

ISBN 978-85-88690-12-7

9 788588 690127

Produced by Mundo Virtual www.mvirtual.com.br

10th International Congress of the Brazilian Geophysical Society

Rio de Janeiro, Brazil
InterContinental Hotel
November 19-23, 2007

10th International Congress of the Brazilian Geophysical Society & EXPOGEF

Unveiling the Earth

Expanded Abstracts

PROMOTION:

SBGf

CO-SPONSORS:

SEG

EAGE EUROPEAN ASSOCIATION OF GEOSCIENTISTS & ENGINEERS

10 International Congress of the
Brazilian Geophysical Society
& EXPOGEF
EAGE
Earth
Expanded
Abstracts